Atmos. Chem. Phys. Discuss., https://doi.org/10.5194/acp-2018-358
Manuscript under review for journal Atmos. Chem. Phys.
Discussion started: 6 April 2018


Atmospheric Chemistry and Physics Discussions

# Extreme levels of Canadian wildfire smoke in the stratosphere over central Europe – Part 2: Lidar study of depolarization and lidar ratios at 355, 532, and 1064 nm and of microphysical properties

Moritz Haarig[1], Albert Ansmann[1], Holger Baars[1], Cristofer Jimenez[1], Igor Veselovskii[2], Ronny Engelmann[1], and Dietrich Althausen[1]

[1]Leibniz Institute for Tropospheric Research, Leipzig, Germany
[2]Physics Instrumentation Center of General Physics Institute, Moscow, Russia

*Correspondence to:* A. Ansmann
(albert@tropos.de)

**Abstract.** Extremely high particle extinction coefficients, an order of magnitude higher than after the Mt. Pinatubo eruption in 1991, were measured in the stratosphere over Leipzig, Germany, on 22 August 2017. In a series of two articles, we present our observations of this record-breaking smoke event. In part 1 (Ansmann et al., 2018), we provide an overview of the smoke situation. The particle extinction coefficients reached 500 $Mm^{-1}$ at 532 nm in the lower stratosphere around 15 km height and the smoke-related aerosol optical thickness (AOT) was close to 1.0 around noon. In part 2, we present the optical and microphysical properties of the fire smoke observed in a tropospheric layer from 5–6.5 km height and in a stratospheric layer from 15–16 km height. Three Raman lidars were run at Leipzig after sunset on 22 August. As a highlight, triple-wavelength polarization/Raman lidar measurements of the particle depolarization ratio and extinction-to-backscatter ratio (lidar ratio) at all three important lidar wavelengths of 355, 532, and 1064 nm could be performed. Very different particle depolarization ratios were found in the troposphere and in the stratosphere. The obviously compact and spherical tropospheric smoke particles caused almost no depolarization of backscattered laser radiation at all three wavelength (<3%), whereas the particles in the stratosphere lead to high depolarization ratios of 22% at 355 nm and 18% at 532 nm and a comparably low value of 4% at 1064 nm in the stratosphere. The observed strong wavelength dependence is probably attributed to the narrow size distribution (accumulation mode) of irregularly shaped soot particles and the absence of a smoke coarse mode. The layer mean particle lidar ratios, on the other hand, were 40-45 sr (355 nm), and 65-80 sr (532 nm), and 80-95 sr (1064 nm) in both, the tropospheric and stratospheric layers indicating similar scattering and absorption properties. The 532 nm single scattering albedo was 0.8 in the stratospheric layer. The smoke particles were rather small (effective radius of 0.17 $\mu$m) in the tropospheric layer and much larger (effective radius of 0.32 $\mu$m) in the very dry stratosphere.

## 1 Introduction

In a series of two papers we report on a rather strong Canadian wildfire smoke event. Optically dense aerosol layers crossed central Europe (Leipzig, Germany) on 22 August 2017. Biomass-burning-smoke was detected at almost all heights in the free

Atmos. Chem. Phys. Discuss., https://doi.org/10.5194/acp-2018-358
Manuscript under review for journal Atmos. Chem. Phys.
Discussion started: 6 April 2018


troposphere and lower stratosphere up to 16 km height, about 3-4 km above the local tropopause. Intensive fires combined with pryocumulonimbus formation in western Canada were most probably responsible for these optically thick stratospheric smoke layers. Khaykin et al. (2018) discussed the strength and spread of the fire smoke in the lower stratosphere in August and September 2017 over the northern hemisphere based on spaceborne lidar observations.

As presented in part 1 (Ansmann et al., 2018), the observed stratospheric particle extinction coefficients at 532 nm reached 500 $Mm^{-1}$ at 15-16 km height and were thus about 20 times higher than the maximum stratospheric extinction coefficients observed after the major Mt. Pinatubo eruption in 1991 (Ansmann et al., 1997; Jäger, 2005). In part 1, we summarized Aerosol Robotic Network (AERONET) sun photometer measurements of the aerosol optical thickness (AOT) at Leipzig and Lindenberg (about 180 km to the northeast of Leipzig), satellite AOT observations (MODIS, Moderate Resolution Imaging Spectroradiometer), and lidar observation with focus on the vertical layering of the forest fire smoke on 22 August around noon, when the thickest smoke plumes crossed Leipzig. The smoke-related AOT was almost 1.0 at 532 nm. The life cycle of stratospheric smoke and the potential influence of strong smoke injections into the stratosphere on climate-relevant processes was discussed in part 1 (introduction).

In part 2, we present the nighttime lidar observations and focus on the optical and microphysical properties of the smoke particles in a tropospheric and a stratospheric layer. Three lidars were involved in the measurements. Besides the continuously running 532 nm Polly (*Po*rtab*l*e *l*idar system) (Althausen et al., 2009; Engelmann et al., 2016), already introduced and used in part 1, we switched on our two powerful advanced aerosol lidars: The dual receiver field-of-view (RFOV) multiwavelength polarization/Raman lidar MARTHA (Multiwavelength Tropospheric Raman lidar for Temperature, Humidity, and Aerosol profiling) (Mattis et al., 2003, 2008; Schmidt et al., 2013, 2014; Jimenez et al., 2017) and the triple-wavelength polarization/Raman lidar BERTHA (Backscatter Extinction lidar-Ratio Temperature Humidity profiling Apparatus) (Althausen et al., 2000; Tesche et al., 2011; Haarig et al., 2016, 2017). MARTHA is part of the European Aerosol Research Lidar Network EARLINET (Mattis et al., 2004; Pappalardo et al., 2014), has a powerful laser transmitting in total 1 J per pulse at a repetition rate of 30 Hz and has an 80 cm telescope, and is thus well designed for tropospheric and stratospheric aerosol observations (Mattis et al., 2004, 2008, 2010). BERTHA is to our knowledge worldwide the only lidar which permits the profiling of aerosols in terms of particle linear depolarization ratio and lidar ratio at all three important lidar wavelengths (355, 532, and 1064 nm). BERTHA was designed and optimized for desert dust characterization and participated in a series of dust field campaigns, e.g., at Barbados in 2013 and 2014 in the framework of the Saharan Aerosol Long-Range Transport and Aerosol–Cloud-interaction Experiment SALTRACE (Weinzierl et al., 2017; Haarig et al., 2017).

The measured profiles of particle backscatter and extinction coefficients, the respective extinction-to-backscatter ratio (lidar ratio), and linear depolarization ratio at several wavelengths from the UV to the near IR contain detailed information about the aerosol type (chemical composition, aerosol mixture), size distribution, and shape characteristics of the particles, and thus document this unprecedented smoke event in large detail. The consistency of all measurements with the three lidars corroborate the high overall quality of the entire lidar data set. We found rather different light depolarization features in the tropospheric smoke layer (5-6.5 km height) and in the optically dense stratospheric smoke layer from 15–16 km height as will be discussed in Sect. 3.

Atmos. Chem. Phys. Discuss., https://doi.org/10.5194/acp-2018-358
Manuscript under review for journal Atmos. Chem. Phys.
Discussion started: 6 April 2018


Atmospheric Chemistry and Physics Discussions

The measurements are also of importance for the following reasons: (1) The spectrally resolved optical data sets for stratospheric smoke can be regarded as a new and important contribution to the aerosol-typing library used in lidar remote sensing (Omar et al., 2009; Burton et al., 2012; Groß et al., 2013; Illingworth et al., 2015; Baars et al., 2016, 2017). (2) The obtained smoke optical properties allow a clear distinction between stratospheric smoke and volcanic aerosols. (3) Our multi-wavelength polarization/Raman lidar observations are complementary to the spaceborne lidar observations of the spread of the smoke over the northern hemisphere with CALIOP (Cloud-Aerosol Lidar with Orthogonal Polarization) (Khaykin et al., 2018). The smoke lidar ratios at 532 and 1064 nm can be used to convert the CALIOP smoke backscatter profiles into profiles of the climate-relevant and more interesting smoke extinction coefficients. (4) Spaceborne lidar activities from CALIOP (since 2006, with laser wavelengths of 532 and 1064 nm) to ATLID (Atmospheric Lidar, laser wavelength of 355 nm) of the EarthCARE (Earth Cloud Aerosol and Radiation Explorer) satellite mission (three year mission probably starting after 2020) (Illingworth et al., 2015) will span about 20 years of global aerosol observations. These aerosol observations performed at 355, 532, and 1064 nm need to be harmonized based on multiwavelength lidar observations of all main aerosol types and mixtures. Our triple-wavelength polarization/Raman lidar of particle extinction, depolarization and lidar ratio can contribute in a rather valuable way to this harmonization of long-term spaceborne aerosol lidar data sets.

## 2 Instrumentation

### 2.1 Lidars

In the evening and night of 22 August 2017, we run three lidars at the European Aerosol Research Lidar Network (EARLINET) station Leipzig (51.3°N, 12.4°W, 120 m above sea level). The single-wavelength 532 nm Polly (*Po*rtab*l*e *l*idar s*y*stem) (Engelmann et al., 2016; Baars et al., 2016) measures the total, co-, and cross-polarized elastic backscatter signals at 532 nm, the rotational Raman signals around 532 nm, and the vibrational-rotational Raman signal at 607 nm. Co- and cross-polarized denotes here the plane of polarization with respect to the plane of the linearly polarized laser pulses. The 532 nm Polly allows us to determine height profiles of the particle backscatter coefficient, extinction coefficient, the corresponding extinction-to-backscatter ratio (lidar ratio) and the particle linear depolarization ratio at 532 nm. Specific details to the data analysis are given in Sect. 2.2.

The second Leipzig lidar is the dual receiver field-of-view (RFOV) multiwavelength polarization/Raman lidar MARTHA (Schmidt et al., 2013; Jimenez et al., 2017). This lidar is unique because it measures Raman signals at 532 and 607 nm and polarizatiom-sensitive 532 nm backscatter signals at two RFOVs so that besides aerosol profiles, cloud microphysical properties can be retrieved from measured cloud multiple scattering effects. We used the 532 nm particle depolarization ratio measured with the smaller RFOV in the study presented here. Furthermore, the 355, 532, and 1064 nm particle backscatter coefficients, the 355 and 532 nm extinction coefficient profiles and the corresponding lidar ratio profiles are presented in the result section.

The third Leipzig lidar is the triple-wavelength polarization/Raman lidar BERTHA (Haarig et al., 2016, 2017). BERTHA allows us to measure particle linear depolarization ratios and lidar ratios at all three important lidar wavelengths of 355, 532, and 1064 nm. In the present configuration, the 1064 nm depolarization ratio and the 1064 nm lidar ratio can only be measured



alternatively (not simultaneously). The 1064 nm depolarization sensitive channel (cross-polarized channel) can be substituted by a 1058 nm rotational Raman channel within 20-30 minutes. This procedure includes adjustment and signal optimizing efforts. On 22 August 2017, we first measured the 1058 nm Raman signal profiles (for 2.5 hours) to obtain the 1064 nm extinction profile, and afterwards the cross-polarized 1064 nm signal component (for 40 minutes), needed in the retrieval of the 1064 nm depolarization ratio.

The laser beams of Polly and BERTHA were tilted to an off-zenith angle of 5° in different directions, whereas MARTHA was pointing to the zenith, which leads to horizontal distances between the laser beams of the order of 450-750 m at the base of the tropospheric smoke layer at 5 km height and of 1.3-2 km at the base of the stratospheric layer at 15 km height. However, the good agreement of the results as discussed in Sect. 3 indicated that the smoke layers were obviously horizontally homogeneous on scales of 1–2 km.

### 2.2 Lidar data analysis: optical properties

Details of the determination of the particle optical properties and the uncertainties in the products can be found in the articles mentioned above. An overview of the retrieval methods is given in Ansmann and Müller (2005); Freudenthaler et al. (2009), and Freudenthaler (2016). The Raman lidar method was exclusively used to determine particle backscatter and extinction profiles. The particle backscatter coefficient is obtained from the measured ratio of the elastic backscatter signal to the respective Raman signal. The extinction coefficients are calculated from the Raman signal profile. In the correction of Rayleigh extinction and backscattering effects, temperature and pressure profiles from the GDAS (Global Data Assimilation System) data base are used (GDAS, 2017). The determination of the particle linear depolarization ratio from the volume depolarization ratio (discussed and shown in part 1) is described in detail by Freudenthaler et al. (2009) and Haarig et al. (2017).

In Sect. 3, the lidar results for the time period from 20:45 – 23:15 UTC on 22 August 2017 (shown in Fig. 1 in Sect. 3) are presented and discussed. The lidar signals for the selected time period of 150 minutes were averaged, background-, and overlap-corrected before the optical properties (backscatter and extinction coefficients, depolarization ratios) were computed. This procedure was performed separately and independently for all three lidar data sets. In case of the 1064 nm depolarization ratio observations with BERTHA, we averaged the signals from 23:50 – 00:30 UTC. The signal profiles had to be smoothed afterwards to reduce the impact of signal noise to a tolerable level on the final products. In the case of the backscatter coefficients and the particle depolarization ratio (determined from the profile of the ratio of the cross-polarized to co-polarized elastic backscatter signal component), we smoothed the individual signal profiles with vertical gliding averaging window lengths of 50-100 m (backscatter coefficients, troposphere), 100-250 m (backscatter coefficient, stratosphere), and 200-400 m (depolarization ratio, troposphere and stratosphere).

In the retrieval of the extinction coefficient, a least-squares linear regression method was applied to the respective Raman signal profiles. The regression window length was 750 m (532 nm) to 1200 m (355 nm) in the troposphere and 1200 m for both wavelengths in the stratosphere. To obtain the lidar ratios at 355 and 532 nm, the extinction profiles were combined with the respective backscatter profiles. In this procedure, we applied the optimum-effective-resolution concept (Iarlori et al., 2015;

Atmos. Chem. Phys. Discuss., https://doi.org/10.5194/acp-2018-358
Manuscript under review for journal Atmos. Chem. Phys.
Discussion started: 6 April 2018


Atmospheric Chemistry and Physics Discussions

Mattis et al., 2016) and used a smoothing window length in the backscatter retrieval which was 0.75 of the regression window length in the extinction retrieval.

In the case of the 1064 nm extinction coefficient, coherent extinction profile structures could not be obtained because the 1058 nm Raman signals were too weak and noisy. The retrieval window lengths are indicated by vertical bars in the figures in the result section (Sect. 3). Retrieval window lengths of 750–1500 m in the troposphere and 2500 m in the stratosphere had to be applied to obtain the 1064 nm extinction coefficient values with a reasonably low uncertainty. The retrieval of the 1064 nm lidar ratio by means of these smoothed values is explained in Sect. 3.

Different expressions for the Ångström exponent, a well-established parameter to characterize the spectral dependence of aerosol optical properties, are shown in Sect. 3. The Ångström exponent $a_{x,\lambda_1/\lambda_2}$ =ln$(x_1/x_2)$/ln$(\lambda_2/\lambda_1)$ describe the wavelength dependence of an optical parameter $x$ in the spectral range from wavelength $\lambda_1$ to $\lambda_2$. $x_i$ may be the backscatter coefficient ($x_i = \beta(\lambda_i)$) or the extinction coefficient ($x_i = \sigma(\lambda_i)$) or the lidar ratio ($x_i = S(\lambda_i)$). The following relationship holds between the backscatter-related, extinction-related and lidar-ratio-related Ångström exponent: $a_{\sigma,\lambda_1/\lambda_2}$ = $a_{\beta,\lambda_1/\lambda_2}$ + $a_{S,\lambda_1/\lambda_2}$ (Ansmann et al., 2002).

### 2.3 Lidar data analysis: microphysical properties

An overview of the theoretical background of the lidar inversion method applied to obtain microphysical particle properties such as the particle effective radius, volume and surface area concentrations and refractive index characteristics from the measured optical properties, i.e., from particle backscatter coefficients at 355, 532, and 1064 nm and extinction coefficients at 355 and 532 nm, is given in Ansmann and Müller (2005). In the present smoke data analysis, we use the method developed by Veselovskii et al. (2002, 2010). The data analysis assumes spherical smoke particles in the tropospheric layer. In the retrieval of the microphysical properties of stratospheric smoke, spherical as well as spheroidal particles are assumed. The single scattering albedo (SSA) of the smoke particles, presented in the result section (Sect. 3) as well, is computed from the retrieved particle size distribution and the most appropriate refractive index characteristics (real and imaginary parts) used as input in the lidar inversion procedure.

## 3 Observations

### 3.1 Overview

An introduction to the record-breaking Canadian wildfire smoke event on 22 August was given in part 1 (Ansmann et al., 2018). It was shown that the total (tropospheric+stratopsheric) smoke-related AOT at 532 nm reached values close to 1.0 during the noon hours. Smoke was present at all heights in the free troposphere as well as in the lower stratosphere up to 16 km height. An optically dense stratospheric layer extended from 14–16 km height and showed a 532 nm AOT of 0.6.

Figure 1 shows the aerosol layering over Leipzig in the night of 22 August 2017, about 10 hours after the maximum smoke burden occurred over Leipzig. Tropospheric aerosol layers were present from the surface to about 6.5–7 km height in the night.

Atmos. Chem. Phys. Discuss., https://doi.org/10.5194/acp-2018-358
Manuscript under review for journal Atmos. Chem. Phys.
Discussion started: 6 April 2018




The top of the planetary boundary layer (PBL) was at 1.8 km height. Between 8 and 13-14 km height, the atmosphere was almost free of smoke. A strong smoke layer is visible between 15 and 16 km, traces of smoke occurred also between 14 and 15 km height. The stratospheric layer was about 3–4 km above the tropopause. The 532 nm AOT of the stratospheric layer had decreased from 0.6 around noon to 0.2–0.25 in the night of 22 August 2017.

### 3.2 Smoke profiling with three lidars

In Figs. 2 and 3, the results of the observations with our three polarization/Raman lidars are presented. Mean height profiles of the optical properties for the time period from 20:45–23:15 UTC on 22 August 2017 are shown, except for the 1064 nm depolarization ratio (23:50–0:30 UTC, see Fig. 1, and explanations in Sect. 2.2). Figure 2 shows the smoke optical properties in the tropospheric layer. According to the backward trajectory analysis presented in part 1, the wildfire smoke traveled about 10 days from the fire sources in western Canada to central Europe. Figure 3 contains the respective findings for the stratospheric smoke layer. This aerosol was probably directly lifted into the stratosphere within deep cumulus towers.

As can be seen in Figs. 2 and 3, a good agreement between the observations with BERTHA, MARTHA, and Polly is given for all parameters. Highlight of our lidar measurements are the lidar ratio and depolarization profiles in Figs. 2c, 2e, 3c, and 3e. However, a high impact of signal noise on the retrieved profiles is visible as well. The MARTHA 355 nm extinction profile could be measured up to about 15.3 km only. The high signal noise is due to the fact that we avoided overloading of the photomultipliers (operated in the photon counting mode) so that even the strong near-range signals in the lowest part of the troposphere were properly measured. As a consequence, the signals were comparably weak in the middle and upper troposphere and lower stratosphere and therefore the influence of signal noise likewise high. This measurement strategy was selected to obtain reliable backscatter and extinction profiles almost from the ground to the top of the stratospheric smoke layer so that the full extinction profiles (as well as the integral) is available for comparison with AERONET sun photometer observations.

In the case of the 1064 nm extinction coefficient, we only can show a few values in Figs. 2 and 3. The retrieval window lengths are indicated by vertical bars. The shown 1064 nm extinction coefficients (and the respective lidar ratio) can be interpreted as mean values for these vertical regression-fit intervals. In the case of stratospheric smoke, a regression window length of 2500 m was required to obtain the 1064 nm extinction coefficient as discussed above. However, the vertical extent of the layer was 1250 m only. Because the densest part of the smoke layer was between 15 and 16 km (as indicated by the backscatter coefficient profiles in Fig. 3), we multiplied the 1064 nm extinction coefficient derived for the 2500 m layer (from 14.4–16.9 km) by a factor of 2 to obtain a trustworthy estimate for the main layer from 15–16 km height. This multiplication yields the correct value if extinction by smoke outside the 15–16 km height range is zero. This assumption is reasonably valid as all backscatter coefficient profiles indicate. To obtain finally the 1064 nm lidar ratio, we combined the extinction value for the 1250 m layer with the respective backscatter coefficient computed from signal profiles smoothed with a window length of 937.5m vertical window length according to the effective resolution concept (Iarlori et al., 2015; Mattis et al., 2016).

Atmos. Chem. Phys. Discuss., https://doi.org/10.5194/acp-2018-358
Manuscript under review for journal Atmos. Chem. Phys.
Discussion started: 6 April 2018


Atmospheric Chemistry and Physics Discussions

### 3.2.1 Main findings

The main results can be summarized as follows: The backscatter and extinction profiles and respective Ångström exponents show typical smoke features. For aged Canadian fire smoke a clear and strong backscatter wavelength dependence is usually observed, whereas the wavelength dependence is weak, absent, or even negative in the case of the extinction coefficient in the 355–532 nm spectral range. Consequently, the 355 nm smoke lidar ratio is smaller than the 532 nm smoke lidar ratio. The reason for the different backscatter and extinction wavelength dependencies is probably related to the fact that the particle backscatter coefficient is a complex function of particle shape, size distribution, and composition (aerosol mixture) whereas extinction of light is mainly a function of size distribution and chemical composition (and corresponding absorption and scattering features), and depends only weakly on particle shape properties. The lidar data inversion analysis, discussed in detail below, revealed that a high imaginary part of 0.04 of the refractive index was needed to reproduce the strong backscatter and low extinction wavelength dependence. This means that high absorption by the smoke particles was most probably responsible for the observed different extinction and backscatter-related Ångström exponents. Our findings are in good agreement with laboratory and field studies of smoke optical properties (Renard et al., 2001, 2002, 2005; Zhang et al., 2008; Lewis et al., 2009; Adachi et al., 2010; China et al., 2015).

The most surprising finding is the strong difference between the depolarization spectrum in the tropospheric and stratospheric smoke layers as shown in Figs. 2e and 3e. The depolarization ratios were at all below 3% for tropospheric smoke, a clear indication that the particles were spherical and/or small. In strong contrast, high depolarization ratios of 22% and 18% were observed at 355 and 532 nm, respectively, in the stratosphere. The depolarization ratios was again low (4%) at 1064 nm. Strong depolarization of the transmitted linearly polarized laser radiation points to irregularly shaped particles.

Table 1 provides an overview of the found optical properties of the tropospheric and stratospheric smoke layers. The presented values can be interpreted as layer-mean values. The microphysical properties in Table 2 are obtained by applying the lidar inversion method described in Sect. 2.3 to the extinction coefficients at 355 and 532 nm in Table 1 and the corresponding backscatter coefficients at 355, 532, and 1064 nm computed from the extinction coefficients, lidar ratios, and respective Ångström exponents in Table 1. The particle mass concentrations were computed from the volume concentrations assuming a smoke particle density of 1.35 g $cm^{-3}$ (Reid and Hobbs, 1998). Mass concentrations were 5–6 $\mu$g $m^{-3}$ in the tropospheric layer and much larger with values close to 40 $\mu$g $m^{-3}$ in the stratospheric layer at the nighttime hours. A clear indication for the presence of highly absorbing stratospheric particles is the low SSA of 0.80–0.85 at 532 nm and 1064 nm.

Figure 4 shows the lidar-derived particle mass size distributions which belongs to the results in Table 2 and is also a product of the lidar data inversion analysis. The size distribution for the particle mass concentration is obtained by multiplying the derived volume size distribution with the smoke particle density of 1.35 g $cm^{-3}$. The respective particle mass size distribution derived from the AERONET observation at Lindenberg in the morning of 23 August 2017 is shown for comparison (Holben et al., 1998; AERONET, 2018). The AERONET observation describes the aerosol in the entire vertical column from the surface to the top of the stratopsheric layer. To convert the AERONET column values to stratospheric volume and mass concentrations so that we can compare sun-photometer-derived and lidar-derived stratospheric volume and mass concentrations, we assumed

Atmos. Chem. Phys. Discuss., https://doi.org/10.5194/acp-2018-358
Manuscript under review for journal Atmos. Chem. Phys.
Discussion started: 6 April 2018


Atmospheric Chemistry and Physics Discussions

that (a) the stratospheric smoke contributed 60% to the total AOT (as observed with lidar) and thus to the column volume concentration, and (b) that these 60% can be assigned to the 1 km thick stratospheric layer from 15 and 16 km height. With this information, the AERONET column volume values for each size bin were converted into volume and mass concentrations as shown in Fig. 4 and interpreted as the stratospheric contribution to the total column mass size distribution.

The lidar-derived and AERONET-derived mass size distributions in Fig. 4 provide a consistent picture of the smoke-related tropospheric and stratospheric size distributions. The pronounced accumulation mode in the AERONET column observation is clearly caused by stratospheric smoke particles. The coarse-mode of the AERONET size distribution is most probably the result of light extinction by boundary-layer aerosol particles (surface soil dust, road dust). By comparing the tropospheric and stratospheric size distributions we see that the particles were comparably small in the tropospheric layer. The size distribution in the stratosphere in Fig. 4 is in good agreement with airborne in situ smoke observations (Fiebig et al., 2002; Petzold et al., 2007; Dahlkötter et al., 2014).

The lidar inversion results in Table 2 and the size distribution in Fig. 4 do not change much when assuming spheroidal instead of spherical particles in the lidar inversion procedure. We hypothesize that the reason for the low impact of particle shape on the retrieval products is the absence of a particle coarse mode in the stratospheric smoke layer so that the particles were at all likewise small. At these conditions shape aspects have a low impact on the lidar inversion products.

### 3.3 Spectral smoke depolarization and lidar ratios

Figure 5 highlights the most important result. The shown depolarization and lidar ratio values are taken from Figs. 2 and 3. A very different spectral behavior was found in the case of the particle linear depolarization ratio in the tropospheric and the stratospheric layer (Fig. 5b), whereas the lidar ratios showed quite similar values and a similar wavelength dependence in both layers (Fig. 5a). As mentioned, the particle depolarization ratio was low at all three wavelengths in the tropospheric layer. These low depolarization values are indicative for spherical or almost spherical particles. The particles must have been compact in shape and many of them may have been composed of a solid soot core with liquid sulfate shell (Dahlkötter et al., 2014). The influence of the shape variability from spherical to rather irregular shaped smoke particles on the optical and radiative properties are discussed by Zhang et al. (2008); Adachi et al. (2010); China et al. (2015). The slightly enhanced tropospheric depolarization values of 2–3% at 355 and 532 nm may have been partly caused by traces of soil dust injected into the atmosphere by the hot fires and associated strong and turbulent winds at the ground (Nisantzi et al., 2014).

In contrast to the tropospheric depolarization ratio spectrum, high depolarization ratios were observed at 355 nm and 532 nm and a strong wavelength dependence were found in the stratospheric layer. The particles were clearly non-spherical. The strong differences between the tropospheric and stratospheric smoke were confirmed by the triple-wavelength polarization lidar observation at Lille, northern France, performed during the same smoke period in August 2017 (Hu et al., 2018). They measured values around 23% (355 nm), 20% (532 nm), and 5% (1064 nm) on 24 August 2017. Furthermore, Burton et al. (2015) observed a rather similar wavelength dependence in a well-defined layer of wildfire smoke advected from the Pacific Northwest of the United States to the Boulder-Denver region at 8 km height. They found depolarization ratios of 21% (355 nm), 9% (532 nm), and 1% (1064 nm) in 8 km height.

Atmos. Chem. Phys. Discuss., https://doi.org/10.5194/acp-2018-358
Manuscript under review for journal Atmos. Chem. Phys.
Discussion started: 6 April 2018


Atmospheric Chemistry and Physics Discussions

In contrast to the strongly different behavior of the depolarization ratio, the lidar ratio spectrum was found to be rather similar in the tropospheric and stratospheric smoke layers. The same origin of the aerosol and thus similar aerosol composition resulting in similar basic scattering and absorption properties may be the reason for the less variable lidar ratios in the tropospheric and stratospheric layers. However, it remains an open question why the difference in the shape characteristics does not have a noticable influence on the lidar ratio spectrum.

The observed mono-modal smoke particle size distributions, i.e., the absence of a coarse mode, is probably the key to understand the found similarities and differences in the tropospheric and stratospheric lidar ratio and depolarization ratio spectra. We hypothesize that the smoke particles were too small to have an impact on the extinction-to-backscatter ratio via different shape properties. A significant impact of the particle shape on the lidar ratio is for example given in the case of desert dust when coarse-mode particles (particles with diameter $>1$ $\mu$m) control the optical effects. Spherical coarse dust particles would cause a lidar ratio around 20 sr, the irregular shape of the particles however leads to lidar ratios of about 50 sr because of a strongly reduced backscatter efficiency of the irregularly shaped dust particles (Mattis et al., 2002).

On the other hand, the aged accumulation-mode smoke was at least able to significantly depolarize laser light by about 20%. This aspect was already discussed in part 1 (Ansmann et al., 2018). The found smoke depolarization-ratio wavelength spectrum is very similar to the one for fine-mode mineral dust. According to Mamouri and Ansmann (2017), which based their discussions on laboratory studies of Järvinen et al. (2016), fine-mode dust causes depolarization ratios of 20–22% (355 nm), 14-17% (532 nm) and $<$10% (1064 nm). The spectral behavior as shown in Fig. 5b is no longer visible when coarse-mode dust particles dominate the depolarization features (Haarig et al., 2017).

The irregular shape of the smoke particles in the stratosphere is partly the result of the very low RH values (of 1% according to the Lindenberg radiosonde profiles between 13 and 17 km height) so that the smoke particles dried out, lost most of the liquid aerosol components, and thus the potential to form a compact particle with spherical shape. Pictures of black carbon aerosol particles taken at 18–21 km height corroborate the irregular shape of stratospheric soot particles (Strawa et al., 1999).

At the end it should be mentioned that also in the case of the stratospheric smoke we can not exclude that soil dust reached stratospheric heights together with the smoke and thus were partly responsible for the enhanced depolarization ratios (Nisantzi et al., 2014). However, the single scattering albedo values derived from the lidar observation point to values around 0.8 at 532 nm (see Table 2) which clearly indicates the dominance of soot particles.

### 3.4 Smoke depolarization and lidar ratios: an updated literature review

Numerous articles on biomass-burning smoke are available in the literature. Multiwavelength lidar studies of fire smoke are presented by, e.g., Wandinger et al. (2002); Murayama et al. (2004); Mattis et al. (2003); Müller et al. (2005); Tesche et al. (2011); Alados-Arboledas et al. (2011); Baars et al. (2012); Nicolae et al. (2013); Pereira et al. (2014); Burton et al. (2015); Veselovskii et al. (2015, 2017); Giannakaki et al. (2015); Ortiz-Amezcua et al. (2017), and Hu et al. (2018). Our literature review is summarized in Table 3 and considers multiwavelength lidar observations only. It was already noticed more than 10 years ago that the 355 nm lidar ratio for aged smoke after many days of long-range transport is considerably lower than the 532 nm lidar ratio (Müller et al., 2005). This is consistent with the discussion and the findings presented above. As can be seen



in Table 3, the difference between the 355 and 532 nm lidar ratios can be as large as 15–25 sr. For fresh smoke, advected from fire sources to the lidar stations within less than 2–3 days, the lidar ratios at 355 and 532 nm are similar or the 355 nm values are larger.

Only a few observations of the particle depolarization ratio in aged and fresh smoke are available as can be seen in Table 3. The low values are indicative for small and spherical smoke particles and moderately increased depolarization ratio may be related to the presence of some soil dust in the smoke plumes or that the smoke particles were partly irregularly in shape. The high depolarization ratios at 355 and 532 nm and the strong wavelength dependence of the depolarization ratio as observed in the August 2017 stratospheric smoke layers are a relatively new features and were first observed in an elevated aged smoke layer in the upper troposphere by Burton et al. (2015).

## 4 Conclusions

An extreme fire smoke event with aerosol layers in the troposphere and stratosphere permitted us to characterize Canadian wildfire smoke after long-range transport in large detail. We used this unprecedented event also to demonstrate the unique potential of our triple-wavelength polarization/Raman lidar to contribute to atmospheric aerosol research. As described in part 1 (Ansmann et al., 2018), the stratospheric particle extinction coefficients reached 500 $Mm^{-1}$ and were thus a factor of 20 higher than the maximum light-extinction coefficients measured over Germany after the major Pinatubo eruption in 1991. The smoke-related AOT was 0.9 at 532 nm on 22 August 2017 as observed with lidar and corroborated by AERONET and MODIS observations. The peak mass concentration of the smoke particles were estimated to be 70–100 $\mu g\ m^{-3}$ in the stratosphere.

In part 2, we focused on the optical and microphysical properties of the fire smoke in two pronounced layers in the troposphere and stratosphere. Three lidars were involved in the studies. Particle backscatter and extinction coefficients, respective lidar ratios, and linear depolarization ratios at all three lidar wavelengths were measured and allowed us to derive microphysical, morphological, and composition-related information about the smoke layers. Very different smoke properties were observed in the tropospheric and stratospheric smoke layers. Very low depolarization ratios (<3% at all three wavelengths) were found in the troposphere (reflecting the predominance of spherical smoke particles), whereas the particles in the stratosphere lead to high depolarization ratios of 22% at 355 nm and 18% at 532 nm and a comparably low value of 4% at 1064 nm in the stratosphere. It was concluded that the strong wavelength dependence is attributed to the narrow size distribution (accumulation mode) of irregularly shaped soot particles and the absence of a smoke particle coarse mode. The layer mean particle lidar ratios, on the other hand, were 40-45 sr (355 nm), and 65-80 sr (532 nm), and 80-95 sr (1064 nm) in both layers which may be an indication for a similar chemical composition of the smoke in the troposphere and stratosphere and thus similar scattering and absorption properties. The single scattering albedo was estimated to be 0.8 at 532 nm in the stratosphere, a clear indication for the presence of soot. The smoke particles were rather small (effective radius of 0.17 $\mu$m) in the tropospheric layer and much larger (effective radius of 0.32 $\mu$m) in the stratosphere.

The spectrally resolved optical data sets for stratospheric smoke can be regarded as an important new contribution to the aerosol-typing library used in lidar remote sensing (Omar et al., 2009; Burton et al., 2012; Groß et al., 2013; Illingworth et al.,



2015; Baars et al., 2016, 2017). The presented optical properties of stratospheric smoke enable a clear and unambiguous discrimination of biomass burning smoke and volcanic aerosol in the stratosphere, and thus to identify and separate these major contributors to stratospheric aerosol perturbations.

The presented triple-wavelength lidar observations are of great value for spaceborne lidar data analysis (harmonization of long-term observations, aerosol trend analysis). NASA's CALIOP (in space since 2006) is operated at 532 and 1064 nm, whereas ATLID of the EarthCARE mission will measure aerosol optical properties at 355 nm. The data harmonization efforts require 1064-nm-to-532-nm, 1064-nm-to-355-nm, 532-nm-to-355-nm conversion factors for backscatter, extinction, and particle depolarization ratio for all important aerosol types and frequently occurring aerosol mixtures. Lidar ratios for 355, 532, and 1064 nm are needed as well. Our smoke lidar-ratio observations at 532 and 1064 nm can already be used in the present CALIOP data analysis of the 2017 smoke event (Khaykin et al., 2018) to estimate smoke extinction coefficients from the measured backscatter profiles.

The unique Canadian wildfire season 2017 can be regarded as a rather favorable opportunity to test atmospheric transport models which consider biomass burning smoke. Especially transport, removal, upward motion of soot particles, and the impact of stratospheric smoke on ice cloud formation, radiative fluxes and chemical processes must be properly modeled to permit state-of-the-art future-climate-change studies. Never before, so many smoke observations with ground-based lidars, organized in several well-organized networks (including EARLINET) were available for intensive model-observation comparisons. Together with the spaceborne CALIOP observations the spread of the smoke over the northern hemisphere is well documented for the year 2017.

As an outlook, in the next step of our studies of the 2017 stratospheric smoke layers over Europe, all PollyNET and EARLINET lidar observations since the summer of 2017 will be analyzed. Smoke layers were observed over whole Europe for several months. Aging of the smoke particles and associated changes in the optical and microphysical properties will be investigated (Baars et al., 2018b). We will also carefully analyze the lidar observations regarding the noticed apparent ascent of the smoke layers from heights of 15–17 km to heights of 23–27 km (Baars et al., 2018a) which is most probably caused by gravito-photophoresis forces (Renard et al., 2008).

## 5 Data availability

The lidar data are available at TROPOS upon request (info@tropos.de). AERONET sun photometer data are downloaded from the AERONET web page (AERONET, 2018).

*Acknowledgements.* We are grateful to AERONET for providing high quality sun photometer observations, calibrations, and products. Special thanks to the Lindenberg AERONET team to carefully run the station. This activity is supported by ACTRIS Research Infrastructure (EU H2020-R&I) under grant agreement no. 654109. The development of the lidar inversion algorithm was supported by the Russian Science Foundation (project 16-17-10241).



## References

Adachi, K., Chung, S. H., and Buseck, P. R.: Shapes of soot aerosol particles and implications for their effects on climate, J. Geophys. Res., 115, D15206, doi:10.1029/2009JD012868, 2010.

AERONET: AERONET aerosol data base, available at: http://aeronet.gsfc.nasa.gov/, last access: 20 February, 2018.

Alados-Arboledas, L., Müller, D, Guerrero-Rascado, J. L., Navas-Guzmán, F., Pérez-Ramírez, D., and Olmo, F. J.: Optical and microphysical properties of fresh biomass burning aerosol retrieved by Raman lidar, and star-and sun-photometry, Geophys. Res. Lett., 38, L01807, doi:10.1029/2010GL045999, 2011.

Althausen, D., Müller, D., Ansmann, A., Wandinger, U., Hube, H., Clauder, E., and Zörner, S.: Scanning six-wavelength eleven channel aerosol lidar, J. Atmos. Ocean. Tech.., 17, 1469–1482, doi:10.1175/1520-0426(2000)017<1469:SWCAL>2.0.CO;2, 2000.

Althausen, D., Engelmann, R., Baars, H., Heese, B., Ansmann, A., Müller, D., and Komppula, M.: Portable Raman Lidar PollyXT for Automated Profiling of Aerosol Backscatter, Extinction, and Depolarization, J. Atmos. Oceanic Tech., 26, 2366-2378, doi:10.1175/2009JTECHA1304.1, 2009.

Ansmann, A. and Müller, D.: Lidar and atmospheric aerosol particles, in: Lidar — Range-Resolved Optical Remote Sensing of the Atmosphere, edited by: Weitkamp, C., Springer Series in Optical Sciences, New York, 105-141, doi:10.1007/0-387-25101-4_4, 2005.

Ansmann, A., Mattis, I., Wandinger, U., Wagner, F. Reichardt, J., and Deshler, T.: Evolution of the Pinatubo Aerosol: Raman Lidar Observations of Particle Optical Depth, Effective Radius, Mass, and Surface Area over Central Europe at 53.48°N, J. Atmos. Sci., 54, 2630–2641, https://doi.org/10.1175/1520-0469(1997)054<2630:EOTPAR>2.0.CO;2, 1997.

Ansmann, A., Wagner, F., Müller, D., Althausen, D., Herber, A., von Hyoningen–Huene, W., and Wandinger, U.: European pollution outbreaks during ACE 2: Optical particle properties inferred from multiwavelength lidar and star–Sun photometry, J. Geophys. Res., 107, doi = 10.1029/2001JD001109, 2002.

Ansmann, A., Baars, H., Haarig, M., Chudnovsky, A., Veselovskii, I., Mattis, I., Seifert, P., and Wandinger, U.: Extreme levels of Canadian wildfire smoke in the stratosphere over central Europe – Part 1: AERONET, MODIS and lidar observations, ACP, submitted, 2018.

Baars, H., Ansmann, A., Althausen, D., Engelmann, R., Heese, B., Müller, D., Artaxo, P., Paixao, M., Pauliquevis, T., and Souza, R.: Aerosol profiling with lidar in the Amazon Basin during the wet and dry season, J. Geophys. Res., 117, D21201, doi:10.1029/2012JD018338, 2012.

Baars, H., Kanitz, T., Engelmann, R., Althausen, D., Heese, B., Komppula, M., Preißler, J., Tesche, M., Ansmann, A., Wandinger, U., Lim, J.-H., Ahn, J. Y., Stachlewska, I. S., Amiridis, V., Marinou, E., Seifert, P., Hofer, J., Skupin, A., Schneider, F., Bohlmann, S., Foth, A., Bley, S., Pfüller, A., Giannakaki, E., Lihavainen, H., Viisanen, Y., Hooda, R. K., Pereira, S. N., Bortoli, D., Wagner, F., Mattis, I., Janicka, L., Markowicz, K. M., Achtert, P., Artaxo, P., Pauliquevis, T., Souza, R. A. F., Sharma, V. P., van Zyl, P. G., Beukes, J. P., Sun, J., Rohwer, E. G., Deng, R., Mamouri, R.-E., and Zamorano, F.: An overview of the first decade of PollyNET: an emerging network of automated Raman-polarization lidars for continuous aerosol profiling, Atmos. Chem. Phys., 16, 5111-5137, doi:10.5194/acp-16-5111-2016, 2016.

Baars, H., Seifert, P., Engelmann, R., and Wandinger, U.: Target categorization of aerosol and clouds by continuous multiwavelength-polarization lidar measurements, Atmos. Meas. Tech., 10, 3175-3201, https://doi.org/10.5194/amt-10-3175-2017, 2017.

Baars et al., Upward transport of stratospheric smoke from Canadian forest fires, to be submitted to ACP, as contribution to the EARLINET special issue, 2018a.

Baars et al., Tropospheric and stratospheric smoke over Europe as observed within EARLINET/ACTRIS in the summer of 2017, to be submitted to ACP, as contribution to the EARLINET special issue, 2018b.

Burton, S. P., Ferrare, R. A., Hostetler, C. A., Hair, J. W., Rogers, R. R., Obland, M. D., Butler, C. F., Cook, A. L., Harper, D. B., and Froyd, K. D.: Aerosol classification using airborne High Spectral Resolution Lidar measurements – methodology and examples, Atmos. Meas. Tech., 5, 73-98, https://doi.org/10.5194/amt-5-73-2012, 2012.

Burton, S. P., Hair, J. W., Kahnert, M., Ferrare, R. A., Hostetler, C. A., Cook, A. L., Harper, D. B., Berkoff, T. A., Seaman, S. T., Collins, J. E., Fenn, M. A., and Rogers, R. R.: Observations of the spectral dependence of linear particle depolarization ratio of aerosols using NASA Langley airborne High Spectral Resolution Lidar, Atmos. Chem. Phys., 15, 13453-13473, doi:10.5194/acp-15-13453-2015, 2015.

China, S., Scarnato, B., Owen, R. C., Zhang, B., Ampadu, M. T., Kumar, S., Dzepina, K., Dziobak, M. P., Fialho, P., Perlinger, J. A., Hueber, J., Helmig, D., Mazzoleni, L. R., and Mazzoleni, C.: Morphology and mixing state of aged soot particles at a remote marine free troposphere site: Implications for optical properties, Geophys. Res. Lett., 42, 1243–1250, doi: 10.1002/2014GL062404, 2015.

Dahlkötter, F., Gysel, M., Sauer, D., Minikin, A., Baumann, R., Seifert, P., Ansmann, A., Fromm, M., Voigt, C., and Weinzierl, B.: The Pagami Creek smoke plume after long-range transport to the upper troposphere over Europe – aerosol properties and black carbon mixing state, Atmos. Chem. Phys., 14, 6111–6137, https://doi.org/10.5194/acp-14-6111-2014, 2014.

Engelmann, R., Kanitz, T., Baars, H., Heese, B., Althausen, D., Skupin, A., Wandinger, U., Komppula, M., Stachlewska, I. S., Amiridis, V., Marinou, E., Mattis, I., Linné, H., and Ansmann, A.: The automated multiwavelength Raman polarization and water-vapor lidar PollyXT: the neXT generation, Atmos. Meas. Tech., 9, 1767-1784, doi:10.5194/amt-9-1767-2016, 2016.

Fiebig, M., Petzold, A., Wandinger, U., Wendisch,M., Kiemle, C., Stifter, A., Ebert, M., Rother, T., and Leiterer, U.: Optical closure for an aerosol column: Method, accuracy, and inferable properties applied to a biomass-burning aerosol and its radiative forcing, J. Geophys. Res., 107, 8130, doi:10.1029/2000JD000192, 2002.

Freudenthaler, V.: About the effects of polarising optics on lidar signals and the $\Delta 90$ calibration, Atmos. Meas. Tech., 9, 4181-4255, https://doi.org/10.5194/amt-9-4181-2016, 2016.

Freudenthaler, V., Esselborn, M., Wiegner, M., Heese, B., Tesche, M., Ansmann, A., Müller, D., Althausen, D., Wirth, M., Fix, A., Ehret, G., Knippertz, P., Toledano, C., Gasteiger, J., Garhammer, M., and Seefeldner, M.: Depolarization ratio profiling at several wavelengths in pure Saharan dust during SAMUM 2006, Tellus B, 61, 165–179, doi:10.1111/j.1600-0889.2008.00396.x, 2009.

GDAS: Global Data Assimilation System, meteorological data base, available at: https://www.ready.noaa.gov/gdas1.php, last access: 20 February, 2018.

Giannakaki, E., Pfüller, A., Korhonen, K., Mielonen, T., Laakso, L., Vakkari, V., Baars, H., Engelmann, R., Beukes, J. P., Van Zyl, P. G., Josipovic, M., Tiitta, P., Chiloane, K., Piketh, S., Lihavainen, H., Lehtinen, K. E. J., and Komppula, M.: One year of Raman lidar observations of free-tropospheric aerosol layers over South Africa, Atmos. Chem. Phys., 15, 5429–5442, doi:10.5194/acp15-5429-2015, 2015.

Groß, S., Esselborn, M., Weinzierl, B., Wirth, M., Fix, A., and Petzold, A.: Aerosol classification by airborne high spectral resolution lidar observations, Atmos. Chem. Phys., 13, 2487-2505, doi:10.5194/acp-13-2487-2013, 2013.

Haarig, M., Engelmann, R., Ansmann, A., Veselovskii, I., Whiteman, D. N., and Althausen, D.: 1064 nm rotational Raman lidar for particle extinction and lidar-ratio profiling: cirrus case study, Atmos. Meas. Tech., 9, 4269-4278, doi:10.5194/amt-9-4269-2016, 2016.

Haarig, M., Ansmann, A., Althausen, D., Klepel, A., Groß, S., Freudenthaler, V., Toledano, C., Mamouri, R.-E., Farrell, D. A., Prescod, D. A., Marinou, E., Burton, S. P., Gasteiger, J., Engelmann, R., and Baars, H.: Triple-wavelength depolarization-ratio profiling of Saharan dust over Barbados during SALTRACE in 2013 and 2014, Atmos. Chem. Phys., 17, 10767–10794, https://doi.org/10.5194/acp-17-10767-2017, 2017.

Holben, B. N., Eck, T. F., Slutsker, I., Tanré, D., Buis, J. P., Setzer, A., Vermote, E., Reagan, J. A., Kaufman, Y. J., Nakajima, T., Lavenu, F., Jankowiak, I., and Smirnov, A.: AERONET – a federated instrument network and data archive for aerosol characterization, Remote Sens. Environ., 66, 1–16, 1998.

Hu, Q., Bravo Aranda, J.-A., Popovici, I., Goloub, P., Povdin, T., Veselovskii, I., Haeffelin, M., and Pitras, C.: Oberservations and analysis of UTLS aerosols detected over northern France, J. Geophys. Res., in revision, 2018.

Iarlori, M., Madonna, F., Rizi, V., Trickl, T., and Amodeo, A.: Effective resolution concepts for lidar observations, Atmos. Meas. Tech., 8, 5157-5176, https://doi.org/10.5194/amt-8-5157-2015, 2015.

Illingworth, A. J., Barker, H. W., Beljaars, A., Ceccaldi, M., Chepfer, H., Clerbaux, N., Cole, J., Delanoe, J., Domenech, C., Donovan, D. P., Fukuda, S., Hirakata, M., Hogan, R. J., Hünerbein, H., Kollias, P., Kubota, T., Nakajima, T., Nakajima, T. Y., Nishizawa, T., Ohno, Y., Okamoto, H., Oki, R., Sato, K., Satoh, M., Shephard, M., Velázquez-Blázquez, A., Wandinger, U., Wehr, T., and Zadelhoff, G.-J.: THE EARTHCARE SATELLITE: the next step forward in global measurements of clouds, aerosols, precipitation and radiation, B. Am. Meteorol. Soc., 96, 1311–1332, doi:10.1175/BAMS-D-12-00227.1, 2015.

Jäger, H.: Long-term record of lidar observations of the stratospheric aerosol layer at Garmisch-Partenkirchen, J. Geophys. Res., 110, D08106, doi:10.1029/2004JD005506, 2005.

Järvinen, E., Kemppinen, O., Nousiainen, Kociok, T., Möhler, O., Leisner, T., and Schnaiter, M.: Laboratory investigations of mineral dust near-backscattering depolarization ratios, J. Quant. Spect. Radiat. Transfer, 178, 192–208, doi:10.1016/j.jqsrt.2016.02.003.

Jimenez, C., Engelmann, R., Donovan, D., Wandinger, U., and Ansmann, A.: Comparison between two Lidar methods to retrieve microphysical properties of liquid-water clouds, Proceeding 28th International Laser Radar Conference, 25-30 June 2017, Bukarest, 2017.

Khaykin, S. M., Godin-Beekmann, S., Hauchecorne, A., Pelon, J., Ravetta, F., and Keckut, P.: Stratospheric smoke with unprecedentedly high backscatter observed by lidars above southern France, Geophys. Res. Lett., 45, https://doi.org/10.1002/2017GL076763, 2018.

Lewis, K. A., Arnott, W. P., Moosmüller, H., Chakrabarty, R. K., Carrico, C. M., Kreidenweis, S. M., Day, D. E., Malm, W. C., Laskin, A., Jimenez, J. L., Ulbrich, I. M., Huffman, J. A., Onasch, T. B., Trimborn, A., Liu, L., and Mishchenko, M. I.: Reduction in biomass burning aerosol light absorption upon humidification: roles of inorganically-induced hygroscopicity, particle collapse, and photoacoustic heat and mass transfer, Atmos. Chem. Phys., 9, 8949-8966, https://doi.org/10.5194/acp-9-8949-2009, 2009.

Mamouri, R.-E. and Ansmann, A.: Potential of polarization/Raman lidar to separate fine dust, coarse dust, maritime, and anthropogenic aerosol profiles, Atmos. Meas. Tech., 10, 3403-3427, https://doi.org/10.5194/amt-10-3403-2017, 2017.

Mattis, I., Ansmann, A., Müller, D., Wandinger, U., and Althausen, D.: Dual-wavelength Raman lidar observations of the extinction-to-backscatter ratio of Saharan dust, Geophys. Res. Lett., 29, 1306, doi:10.1029/2002GL014721, 2002.

Mattis, I., Ansmann, A., Wandinger, U., and Müller, D.: Unexpectedly high aerosol load in the free troposphere over Central Europe in spring/summer 2003, Geophys. Res. Lett., 30, 2178, doi:10.1029/2003GL018442, 2003.

Mattis, I., Ansmann, A., Müller, D., Wandinger, U., and Althausen, D.: Multiyear aerosol observations with dual-wavelength Raman lidar in the framework of EARLINET, J. Geophys. Res., 109, D13203, doi:10.1029/2004JD004600, 2004.

Mattis, I., Müller, D., Ansmann, A., Wandinger, U., Preißler, J., Seifert, P., and Tesche, M.: Ten years of multiwavelength Raman lidar observations of free–tropopsheric aerosol layers over central Europe: Geometrical properties and annual cycle, J. Geophys. Res., 113, D20202, doi:10.1029/2007JD009636, 2008.

Mattis, I., Seifert, P., Müller, D., Tesche, M., Hiebsch, A., Kanitz, T., Schmidt, J., Finger, F., Wandinger, U., and Ansmann, A.: Volcanic aerosol layers observed with multiwavelength Raman lidar over central Europe in 2008-–2009, J. Geophys. Res., 115, D00L04, doi:10.1029/2009JD013472, 2010.

Mattis, I., D'Amico, G., Baars, H., Amodeo, A., Madonna, F., and Iarlori, M.: EARLINET Single Calculus Chain – technical – Part 2: Calculation of optical products, Atmos. Meas. Tech., 9, 3009-3029, https://doi.org/10.5194/amt-9-3009-2016, 2016.

Müller, D., Mattis, I., Wandinger, U., Ansmann, A., Althausen, A., and Stohl, A.: Raman lidar observations of aged Siberian and Canadian forest fire smoke in the free troposphere over Germany in 2003: Microphysical particle characterization, J. Geophys. Res., 110, D17201, doi:10.1029/2004JD005756, 2005.

Murayama, T., Müller, D., Wada, K., Shimizu, A., Sekiguchi, M., and Tsukamoto, T.: Characterization of Asian dust and Siberian smoke with multi-wavelength Raman lidar over Tokyo, Japan in spring 2003, Geophys. Res. Lett., 31, L23103, doi:10.1029/2004GL021105, 2004.

Nicolae, D., Nemuc, A., Müller, D., Talianu, C., Vasilescu, J., Belegante, L., and Kolgotin, A.: Characterization of fresh and aged biomass burning events using multiwavelength Raman lidar and mass spectrometry, J. Geophys. Res. Atmos., 118, 2956–2965, doi:10.1002/jgrd.50324, 2013.

Nisantzi, A., Mamouri, R. E., Ansmann, A., and Hadjimitsis, D.: Injection of mineral dust into the free troposphere during fire events observed with polarization lidar at Limassol, Cyprus, Atmos. Chem. Phys., 14, 12155-12165, doi:10.5194/acp-14-12155-2014, 2014.

Omar, A. H., Winker, D. M., Kittaka, C., Vaughan, M. A., Liu, Z., Hu, Y., Trepte, C. R., Rogers, R. R., Ferrare, R. A., Lee, K.-P., Kuehn, R. E., and Hostetler, C. A.: The CALIPSO Automated Aerosol Classification and Lidar Ratio Selection Algorithm, J. Atmos. Ocean. Tech., 26, 1994–2014, https://doi.org/10.1175/2009JTECHA1231.1, 2009.

Ortiz-Amezcua, P., Guerrero-Rascado, J. L., Granados-Muñoz, M. J., Benavent-Oltra, J. A., Böckmann, C., Samaras, S., Stachlewska, I. S., Janicka, L., Baars, H., Bohlmann, S., and Alados-Arboledas, L.: Microphysical characterization of long-range transported biomass burning particles from North America at three EARLINET stations, Atmos. Chem. Phys., 17, 5931-5946, https://doi.org/10.5194/acp-17-5931-2017, 2017.

Pappalardo, G., Amodeo, A., Apituley, A., Comeron, A., Freudenthaler, V., Linné, H., Ansmann, A., Bösenberg, J., D'Amico, G., Mattis, I., Mona, L., Wandinger, U., Amiridis, V., Alados-Arboledas, L., Nicolae, D., and Wiegner, M.: EARLINET: towards an advanced sustainable European aerosol lidar network, Atmos. Meas. Tech., 7, 2389–2409, doi:10.5194/amt-7-2389-2014, 2014.

Pereira, S. N., Preißler, J., Guerrero-Rascado, J. L., Silva, A. M., and Wagner, F.: Forest Fire Smoke Layers Observed in the Free Troposphere over Portugal with a Multiwavelength Raman Lidar: Optical and Microphysical Properties, The Scientific World Journal, 421838, http://doi.org/10.1155/2014/421838, 2014.

Petzold, A., Weinzierl, B., Huntrieser, H., Stohl, A., Real, E., Cozic, J., Fiebig, M., Hendricks, J., Lauer, A., Law, K., Roiger, A., Schlager, H., and Weingartner, E.: Perturbation of the European free troposphere aerosol by North American forest fire plumes during the ICARTT-ITOP experiment in summer 2004, Atmos. Chem. Phys., 7, 5105-5127, doi:10.5194/acp-7-5105-2007, 2007.

Reid, J. S., and Hobbs, P. V.: Physical and optical properties of young smoke from individual biomass fires in Brazil, J. Geophys. Res., 103, 32013-32030, doi:10.1029/98JD00159, 1998.

Renard, J.-B., Hadamcik, E., Brogniez, C., Berthet, G., Worms, J. C., Chartier, M., Pirre, M., Ovarlez, J., and Ovarlez, H.: UV-visible bulk optical properties of randomly distributed soot, Appl. Opt., 40, 6575–6580, doi:10.1364/AO.40.006575, 2001.

Renard, J.-B., Berthet, G., Robert, C., Chartier, M., Pirre, M., Brogniez, C., Herman, M., Verwaerde, C., Balois, J.–Y., Ovarlez, J., Ovarlez, H., Crespin, J., and Deshler, T., Optical and physical properties of stratospheric aerosols from balloon measurements in the visible and near-infrared domains: II. Comparison of extinction, reflectance, polarization and counting measurements, Appl. Opt., 41, 7540–7549, doi:10.1364/AO.41.007540, 2002.

Renard, J.-B., Ovarlez, J., Berthet, G., Fussen, D., Vanhellemont, F., Brogniez, C., Hadamcik, E., Chartier, M., and Ovarlez, H.: Optical and physical properties of stratospheric aerosols from balloon measurements in the visible and near-infrared domains. III. Presence of aerosols in the middle stratosphere, Appl. Opt., 44, 4086 – 4095, doi:10.1364/ AO.44.004086, 2005.

Renard, J.-B., Brogniez, C., Berthet, G., Bourgeois, Q., Gaubicher, B., Chartier, M., Balois, J.-Y., Verwaerde, C., Auriol, F., Francois, P., Daugeron, D., and Engrand, C.: Vertical distribution of the different types of aerosols in the stratosphere: Detection of solid particles and analysis of their spatial variability, J. Geophys. Res., 113, D21303, doi:10.1029/2008JD010150, 2008.

Schmidt, J., Wandinger, U., and Malinka, A.: Dual-field-of-view Raman lidar measurments for the retrieval of cloud microphysical properties, Appl. Opt., 52, 2235-2247, 2013.

Schmidt, J., Ansmann, A., Bühl, J., Baars, H., Wandinger, U., Müller, D., and Malinka, A. V.: Dual-FOV Raman and Doppler lidar studies of aerosol-cloud interactions: Simultaneous profiling of aerosols, warm-cloud properties, and vertical wind, J. Geophys. Res., 119, doi:10.1002/2013JD020424, 2014.

Strawa, A. W., Drdla, K., Ferry, G. V., Verma, S., Pueschel, R. F., Yasuda, M., Salawitch, R. J., Gao, R. S., Howard, S. D., Bui, P. T., Loewenstein, M., Elkins, J. W., Perkins, K. K., and Cohen, R.: Carbonaceous aerosol (soot) measured in the lower stratosphere during POLARIS and its role in stratospheric photochemistry, J. Geophys. Res., 104, 26753–26766, doi:10.1029/1999JD900453, 1999.

Tesche, M., Müller, D., Groß, S., Ansmann, A., Althausen, D., Freudenthaler, V., Weinzierl, B., Veira, A., and Petzold, A.: Optical and microphysical properties of smoke over Cape Verde inferred from multiwavelength lidar measurements. Tellus B, 63, 677–694. doi:10.1111/j.1600-0889.2011.00549.x, 2011.

Veselovskii I., Kolgotin, A., Griaznov, V., Müller, D., Wandinger, U., and Whiteman, D.: Inversion with regularization for the retrieval of tropospheric aerosol parameters from multi-wavelength lidar sounding, Appl. Opt., 41, 3685–699, https://doi.org/10.1364/AO.41.003685, 2002.

Veselovskii, I., Dubovik, O., Kolgotin, A., Lapyonok, T., Di Girolamo, P., Summa, D., Whiteman, D. N., Mishchenko, M. and Tanré, D.: Application of randomly oriented spheroids for retrieval of dust particle parameters from multiwavelength lidar measurements, J. Geophys. Res., 115, D21203, doi:10.1029/2010JD014139, 2010.

Veselovskii, I., Whiteman, D. N., Korenskiy, M., Suvorina, A., Kolgotin, A., Lyapustin, A., Wang, Y., Chin, M., Bian, H., Kucsera, T. L., Pérez-Ramírez, D., and Holben, B.: Characterization of forest fire smoke event near Washington, DC in summer 2013 with multiwavelength lidar, Atmos. Chem. Phys., 15, 1647-1660, https://doi.org/10.5194/acp-15-1647-2015, 2015.

Veselovskii, I., Goloub, P., Podvin, T., Tanre, D., da Silva, A., Colarco, P., Castellanos, P., Korenskiy, M., Hu, Q., Whiteman, D. N., Pérez-Ramírez, D., Augustin, P., Fourmentin, M., and Kolgotin, A.: Characterization of smoke/dust episode over West Africa: comparison of MERRA-2 modeling with multiwavelength Mie-Raman lidar observations, Atmos. Meas. Tech. Discuss., https://doi.org/10.5194/amt-2017-342, in review, 2017.

Wandinger, U., Müller, D., Böckmann, C., Althausen, D., Matthias, V., Bösenberg, J, Weiß, V., Fiebig, M., Wendisch, M., Stohl, A., and Ansmann. A.: Optical and microphysical characterization of biomass-burning and industrial-pollution aerosols from multiwavelength lidar and aircraft measurements, J. Geophys. Res.,107(D21), doi:10.1029/2000JD000202,2002.

Weinzierl, B., Ansmann, A, Prospero, J. M., Althausen, D., Benker, N., Chouza, F., Dollner, M., Farrell, D., Fomba, W. K., Freudenthaler, V., Gasteiger, J., Groß, S., Haarig, M., Heinold, B., Kandler, K., Kristensen, T. B., Mayol-Bracero, O.-L., Müller, T., Reitebuch, O., Sauer, D., Schäfler, A., Schepanski, K., Tegen, I., Toledano, C., Walser, A.: The Saharan Aerosol Long-range TRansport and Aerosol Cloud Interaction Experiment (SALTRACE): overview and selected highlights, Bull. American. Meteorol. Soc., 98, 1-25, doi:10.1175/BAMS-D-15-00142.1, 2017.



Zhang, R., Khalizov, A. F., Pagels, J., Zhang, D., Xue, H., and McMurry, P. H.: Variability in morphology, hygroscopicity, and optical properties of soot aerosols during atmospheric processing, Proc. Natl. Acad. Sci. USA, 105, 10291–10296, doi:10.1073/pnas.0804860105, 2008.

Atmos. Chem. Phys. Discuss., https://doi.org/10.5194/acp-2018-358
Manuscript under review for journal Atmos. Chem. Phys.
Discussion started: 6 April 2018


Atmospheric Chemistry and Physics Discussions

**Table 1.** Optical properties of smoke aerosol in the tropospheric layer (5–6.5 km height) and stratospheric smoke layer (15-16 km height). Layer mean values of the particle extinction coefficient $\sigma$, lidar ratio $S$, linear depolarization ratio $\delta$, and backscatter-related and extinction-related Ångström exponent $a_{\sigma,\lambda_1/\lambda_2}$ and $a_{\beta,\lambda_1/\lambda_2}$ for the wavelength range from $\lambda_1$ to $\lambda_2$ are given. The mean values are based on all lidar observations taken in the night of 22 August 2017.

| **Parameter** | **Troposphere** | | | **Stratosphere** | | |
|---|---|---|---|---|---|---|
| | 355 nm | 532 nm | 1064 nm | 355 nm | 532 nm | 1064 nm |
| $\sigma$ | 60 Mm$^{-1}$ | 42 Mm$^{-1}$ | 28 Mm$^{-1}$ | 200 Mm$^{-1}$ | 225 Mm$^{-1}$ | 125 Mm$^{-1}$ |
| $S$ | 45 sr | 68 sr | 82 sr | 40 sr | 72 sr | 92 sr |
| $\delta$ | 2% | 3% | 1% | 22% | 18% | 4% |
| $a_{\sigma,355/532}$ | | 0.9 | | | -0.3 | |
| $a_{\sigma,532/1064}$ | | | 0.6 | | | 0.85 |
| $a_{\beta,355/532}$ | | 2.1 | | | 1.2 | |
| $a_{\beta,532/1064}$ | | | 0.8 | | | 1.2 |

**Table 2.** Lidar inversion products (assuming spherical particles) for the tropospheric layer (5–6.5 km height) and stratospheric smoke layer (15-16 km height). Layer mean values of the particle volume concentration $V$, mass concentration $m$, effective radius $r_{\text{eff}}$, number concentration $N$, and single scattering albedo SSA are given.

| **Parameter** | **Troposphere** | **Stratosphere** |
|---|---|---|
| $V$ | 4±1.2 $\mu$m$^3$ cm$^{-3}$ | 28±9 $\mu$m$^3$ cm$^{-3}$ |
| $m$ | 5.5±1.8 $\mu$g m$^{-3}$ | 38±12 $\mu$g m$^{-3}$ |
| $r_{\text{eff}}$ | 0.17±0.06 $\mu$m | 0.32±0.10 $\mu$m |
| $N$ | 212±80 cm$^{-3}$ | 323±120 cm$^{-3}$ |
| SSA | | 0.74 (355 nm) |
| | | 0.80 (532 nm) |
| | | 0.83 (1064 nm) |

Atmos. Chem. Phys. Discuss., https://doi.org/10.5194/acp-2018-358
Manuscript under review for journal Atmos. Chem. Phys.
Discussion started: 6 April 2018


Atmospheric Chemistry and Physics Discussions

**Table 3.** Literature overview of multiwavelength lidar observations of smoke lidar ratios and particle linear depolarization ratios of fresh and aged biomass-burning smoke in the troposphere and stratosphere. For better comparison, the tropospheric triple-wavelength depolarization ratio observation of Burton et al. (2015) performed in aged northwestern American smoke is listed in the third line, i.e., before the tropospheric section. The lidar and depolarization ratios of Hu et al. (2018) were measured at Lille, northern France, on 24 August 2017.

| **Study** | **Lidar ratio** | | | **Depolarization ratio** | | |
|---|---|---|---|---|---|---|
| | 355 nm | 532 nm | 1064 nm | 355 nm | 532 nm | 1064 nm |
| **Stratosphere, Canadian smoke** | | | | | | |
| This study, aged | 40±16 sr | 66±12 sr | 92±27 sr | 0.224±0.015 | 0.184±0.006 | 0.043±0.007 |
| Hu et al. (2018), aged | 33±5 sr | 53±8 sr | – | 0.23±0.03 | 0.20±0.03 | 0.05±0.008 |
| Burton et al. (2015), aged | – | – | – | 0.203±0.036 | 0.093±0.015 | 0.018±0.002 |
| **Troposphere, Canadian and Siberian smoke** | | | | | | |
| Wandinger et al. (2002) and | | | | | | |
| Fiebig et al. (2002), aged | 40–70 sr | 40–80 sr | – | – | 0.06–0.11 | – |
| Murayama et al. (2004), aged | 40 sr | 65 sr | – | – | 0.06 | – |
| Müller et al. (2005), aged | 30–55 sr | 40–60 sr | – | – | – | – |
| Veselovskii et al. (2015), fresh | 65–90 sr | 65–80 sr | – | – | – | – |
| Ortiz-Amezcua et al. (2017), aged | 23–34 sr | 47–58 sr | – | – | 0.02–0.08 | – |
| This study, aged | 46±6 sr | 67±4 sr | 82±22 sr | 0.021±0.040 | 0.029±0.015 | 0.009±0.008 |
| Hu et al. (2018), aged | – | 75 sr | – | 0.10±0.02 | 0.05±0.01 | 0.008 ±0.002 |
| **Troposphere, European smoke** | | | | | | |
| Alados-Arboledas et al. (2011) | 60–65 sr | 60–65 sr | – | – | – | – |
| Nicolae et al. (2013) | 73±12 sr | 46±6 sr | – | – | – | – |
| Nicolae et al. (2013), aged | 40±16 sr | 54±10 | – | – | – | – |
| Pereira et al. (2014) | 56±6 sr | 56±6 sr | – | – | 0.05±0.01 | – |
| **Troposphere, Amazonian smoke** | | | | | | |
| Baars et al. (2012), aged | 62±12 sr | 64±15 sr | – | 0.025±0.01 | – | – |
| **Troposphere, African smoke** | | | | | | |
| Tesche et al. (2011) | 87±17 sr | 79±17 sr | – | – | – | – |
| Giannakaki et al. (2015) | 89±20 sr | 83±23 sr | – | – | – | – |

Atmos. Chem. Phys. Discuss., https://doi.org/10.5194/acp-2018-358
Manuscript under review for journal Atmos. Chem. Phys.
Discussion started: 6 April 2018


Atmospheric Chemistry and Physics Discussions

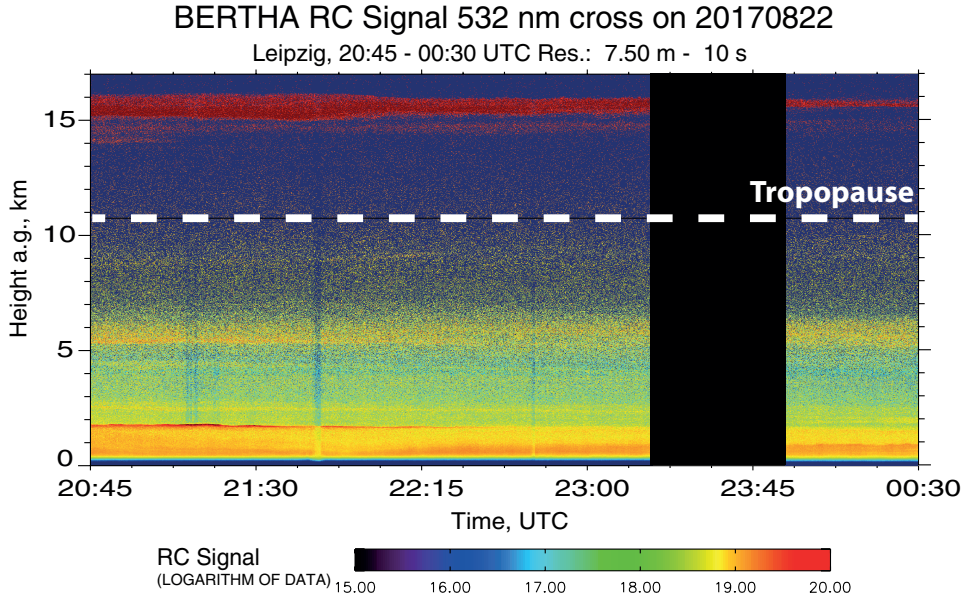


**Figure 1.** Canadian wildfire smoke layers in the troposphere (mostly between boundary-layer top at 1.8 and 6.5 km height) and in the stratosphere (15–16 km height) observed with lidar at Leipzig on 22-23 August 2017, 20:45–00:30 UTC. Shown is the range-corrected cross-polarized 532 nm backscatter signal measured with temporal and vertical resolution of 10 s and 7.5 m, respectively. The indicated tropopause height (GDAS, 2017) is in agreement with nearby radiosonde profiles.

Atmos. Chem. Phys. Discuss., https://doi.org/10.5194/acp-2018-358
Manuscript under review for journal Atmos. Chem. Phys.
Discussion started: 6 April 2018


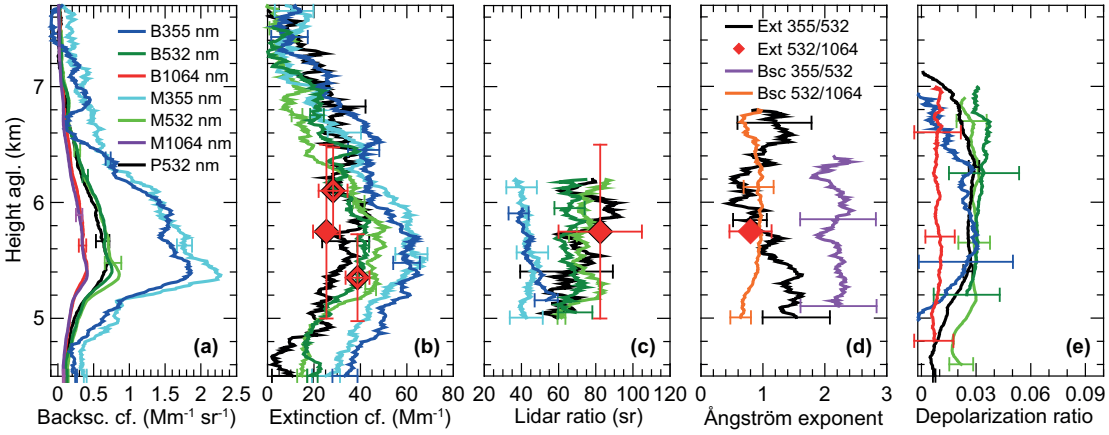


**Figure 2.** 2.5-hour mean profiles (20:45-23:15 UTC, see Fig. 1) of optical properties in the tropospheric smoke layer: (a) particle backscatter coefficient at three wavelengths measured with three lidars (BERTHA, B, MARTHA, M, and 532 nm Polly, P), (b) respective extinction coefficients (colors as in a), (c) extinction-to-backscatter ratio (lidar ratio, colors as in a), (d) backscatter-related (Bsc) and extinction-related (Ext) Ångström exponents (BERTHA only), and (e) particle linear depolarization ratio (colors as in a). Error bars indicate the retrieval uncertainty (one standard deviation). In the case of the 1064 nm extinction coefficient, a height profile could not be determined. Therefore, only a few values for retrieval window length (least-squares method) of 750 and 1500 m (indicated by vertical bars) are shown. The 1064 nm lidar ratio is given for the 1500 m retrieval interval length. The 1064 nm depolarization ratio was measured between 23:50 and 00:30 UTC. For more details, see Sect. 2.2.

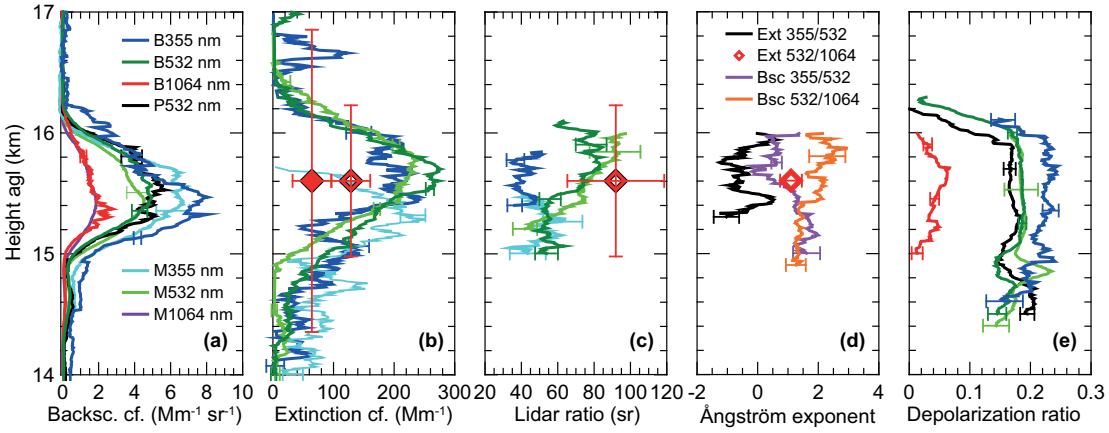


**Figure 3.** Same as Fig. 2, except for the stratospheric aerosol layer and for different signal smoothing lengths (as explained in Sect. 2.2). In the case of the 1064 nm extinction coefficient (red solid diamond) , a retrieval window length (least-squares method) of 2500 m had to be applied (indicated by the long vertical bar). We estimated the layer mean 1064 nm extinction coefficient (red open diamond) for the 1250 m thick layer from 15–16.25 km height by multiplying the obtain value for 2500 window length by a factor of 2, assuming that the extinction below and above the 1250 m thick layer was close to zero. In the subsequently calculation of the 1064 nm lidar ratio we used this 1250 m layer mean extinction value (open diamond) together with an appropriately smoothed backscatter coefficient (see text for more details).

Atmos. Chem. Phys. Discuss., https://doi.org/10.5194/acp-2018-358
Manuscript under review for journal Atmos. Chem. Phys.
Discussion started: 6 April 2018


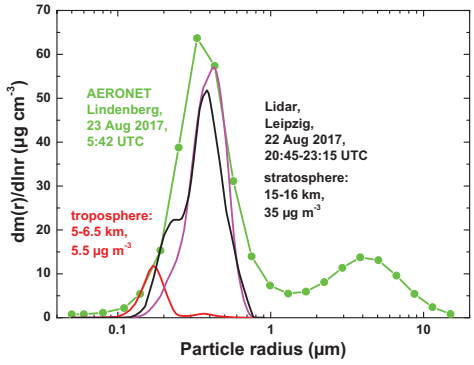


**Figure 4.** Particle mass size distribution derived from column (tropospheric + stratospheric) AERONET observations at Lindenberg, 180 km northeast of the lidar site, in the morning of 23 August 2017 (green) and obtained from the inversion of lidar-derived optical properties in the tropospheric layer (red) and stratospheric layer (black, magenta). Small particles prevailed in the tropospheric layer and comparably large accumulation-mode particles dominated in the stratospheric layer. The black and magenta curves are obtained by assuming spherical and spheroidal particle shapes in the lidar data inversion, respectively.

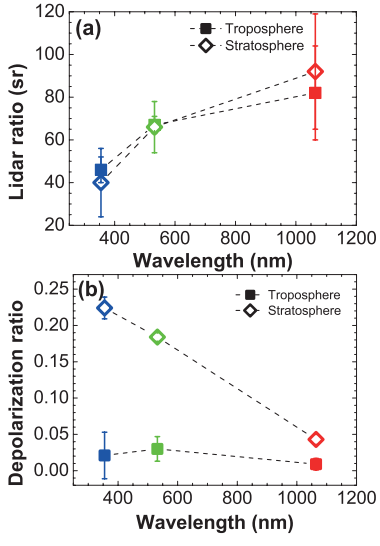


**Figure 5.** Comparison of the spectral dependence of the tropospheric (5-6 km height) and stratospheric (15-16 km height) particle lidar ratio (a) and particle linear depolarization ratio (b). A strongly contrasting spectral behavior is found in the case of the depolarization ratio and an almost similar wavelength dependence (in the troposphere and stratosphere) is found for the lidar ratio. Only BERTHA values are considered.